A New Technique Using Infrared Satellite Measurements to Improve the Accuracy of the CALIPSO Cloud-Aerosol Discrimination Method

Aaron R. Naeger, Sundar A. Christopher, Richard Ferrare, *Member, IEEE*, and Zhaoyan Liu, *Member, IEEE*

***Abstract*—In this paper, we develop a new technique called the brightness temperature difference cloud and aerosol discrimination algorithm (BTD CAD) that uses thermal infrared satellite measurements to improve the accuracy of the cloud-aerosol lidar and infrared pathfinder satellite observations (CALIPSO) CAD algorithm. It has been shown that the CALIPSO CAD algorithm can misclassify dense dust as cloud because the CALIPSO two-wavelength backscatter lidar operates at 532 and 1064 nm where very similar scattering properties are known to exist between dense dust and cloud. Therefore, we use the 11 and 12 μm thermal infrared channels from both the moderate resolution imaging spectroradiometer (MODIS) and the spinning enhanced visible and infrared imager (SEVIRI), which are very sensitive to dust concentration, in order to reduce the frequency of the dust misclassifications encountered by the CALIPSO CAD algorithm. For the two Saharan dust events presented in this paper, both the MODIS and SEVIRI BTD CAD techniques performed well but the MODIS BTD CAD correctly reclassified more CALIPSO CAD misclassifications as dust. After applying both techniques to all the daytime CALIPSO transects over North Africa during June 2007, the MODIS and SEVIRI BTD CAD increased the total number of detected aerosol layers by approximately 10% and 4%, respectively. Even though the Version 3 (V3) CAD algorithm is significantly more accurate in deciphering between dense dust and clouds than the Version 2 algorithm, the V3 still showed some dust misclassifications among the case studies. Thus, the BTD CAD technique can help reduce the frequency of dust misclassifications encountered by the V3 CAD algorithm.**

***Index Terms*—Aerosol, cloud, remote sensing.**

I. Introduction

MUCH uncertainty still exists regarding the influence of aerosols on the global radiation budget and climate [1]. Tropospheric aerosols, such as smoke from biomass burning and dust aerosols, impact the radiative energy budget of the earth-atmosphere system through the aerosol direct, indirect, and semi-direct radiative effects [2]. In cloud-free conditions, dust and smoke aerosols reflect and absorb shortwave radiation, which is known as the shortwave direct radiative effect [3]. Dust aerosols also have an important influence in the longwave since they reduce the amount of longwave radiation by emitting at colder temperatures while absorbing and reemitting longwave radiation back toward the surface [4], [5]. The aerosol indirect radiative effect arises when aerosols interact with clouds causing increased cloud albedo and suppression of precipitation influencing longer cloud lifetimes (e.g., [6]). Additionally, the semi-direct effect occurs when aerosols absorb shortwave radiation and heat the atmosphere which can lead to low-level cloud evaporation [7]. In order to reduce the uncertainties with the aerosol and cloud effects, the type of aerosol, their properties, and their vertical distributions must be known.

Most passive remote sensing sensors such as the moderate resolution imaging spectroradiometer (MODIS) or the multiangle imaging spectroradiometer (MISR) provide columnar information of aerosol properties only in cloud-free conditions. Therefore, when using satellite measurements, the shortwave radiative effect is calculated only in regions without cloud cover [8]. For example, over oceans in the shortwave part of the spectrum, aerosols appear brighter than the surface thereby leading to a negative top of atmosphere radiative effect value [9]. Over land, the direct radiative effect (DRE) value could be either positive or negative depending upon aerosol properties and surface albedo [10]. However, since boundary layer clouds are brighter than the ocean background, the sign of the DRE changes when aerosols reside above clouds, even over ocean surfaces [11]. Therefore, knowledge of the vertical distribution of aerosols is critical.

Unlike passive remote sensing instruments (e.g., MODIS, MISR), the cloud-aerosol lidar and infrared pathfinder satellite observations (CALIPSO) satellite, which carries an active lidar called cloud-aerosol lidar with orthogonal polarization (CALIOP), provides backscatter measurements at two wavelengths (532, 1064 nm) and therefore provides a measure of the vertical distribution of clouds and aerosols during the day and night. The lidar is also polarization sensitive which allows for a classification of dust and smoke aerosols [12]. Where passive remote sensing instruments encounter difficulties over desert regions due to the high surface reflectance, CALIPSO is able to detect atmospheric features, such as

Manuscript received April 11, 2011; revised December 13, 2011 and March 9, 2012; accepted May 15, 2012. This work was supported by NASA's Radiation Science and AURA grants.

A. R. Naeger is with the Department of Atmospheric Sciences, University of Alabama, Huntsville, AL 35805 USA (e-mail: naeger@nsstc.uah.edu).

S. A. Christopher is with the Department of Atmospheric Sciences, University of Alabama, Huntsville, AL 35805 USA and also with Earth System Science Center, University of Alabama, Huntsville, AL 35805 USA (e-mail: sundar@nsstc.uah.edu).

R. Ferrare is with NASA Langley Research Center, Hampton, VA 23666 USA (e-mail: richard.a.ferrare@nasa.gov).

Z. Liu is with National Institute of Aerospace, NASA Langley Research Center, Hampton, VA 23681-2199 USA (e-mail: zhaoyan.liu@nasa.gov).

Color versions of one or more of the figures in this paper are available online at http://ieeexplore.ieee.org.

Digital Object Identifier 10.1109/TGRS.2012.2201161

TABLE I
DESCRIPTION OF THE DATA PRODUCTS USED IN THIS STUDY

Satellite	Data Level / Version	Data Product Name	Horizontal Resolution	Vertical Resolution	Parameters Used
CALIPSO	Level 1B Version 3	CAL_LID_L1-ValStage-V3	333 m (sfc-8.3 km)	30-60 m	1) Attenuated Backscatter
CALIPSO	Level 2 Version 2 & 3 - Aerosol	CAL_LID_L2-05kmAlay	5 km	Up to 8 layers	1) Layer Top Height 2) Integrated Attenuated Backscatter 3) Integrated Volume Depolarization Ratio 4) Integrated Attenuated Total Color Ratio 5) Horizontal Resolution
CALIPSO	Level 2 Version 2 & 3 - Cloud	CAL_LID_L2-05kmClay	5 km	Up to 10 layers	
MSG-2	Level 1.5	MSG15	3 km	NA	1) Radiance
Aqua/MODIS	Level 1B	MYD021KM	250 m - 1 km	NA	1) Radiance
Cloudsat	Level 2B	GEOPROF	1.3 x 1.7 km	NA	1) CPR Cloud Mask

aerosols [13]. Although the CALIPSO satellite provides unique advantages over passive remote sensing instruments, day/night signal differences may cause uncertainty with CALIPSO data. Due to the solar background signal present during the daytime, the background noise is higher, and thus the signal-to-noise ratio is lower than the nighttime CALIPSO transects [14]. In addition, the ratio of the 1064-nm and 532-nm-high cloud signals shows a time-varying nonlinear dependence on latitude for the daytime sections, indicating that sunlight introduces different thermal effects on the two channels [14]. However, during the daylight orbit segment, a constant scaling factor is computed in the current Version 3 (V3) release to transfer the 532-nm calibration coefficients to the 1064-nm channel, so that the 1064-nm calibration coefficient is the product of this constant scaling factor and a latitudinally varying 532-nm calibration coefficient [15], [16]. Therefore, the color ratio (1064/532 nm channels) is less accurate (usually larger for the daytime data than nighttime data), and this study uses daytime CALIPSO data where these larger uncertainties are generally present. Also, due to the differing detector transient response and multiple scattering effects of the two channels in dense layers, the detection of any aerosol and cloud layers beneath dense layers (optical depth $>\sim 2.5$) is highly uncertain [12].

Global dust emissions have been estimated to range from 1000 to 3000 Tg per year with over 50% originating from Africa due to the immense Sahara Desert residing in North Africa [17]. A commonly used technique to identify dust over the desert is the difference in temperatures between the 11 and 12 μm channel (BTD). Negative BTD11-12 is often observed for dense dust plumes because dust has a larger imaginary index of refraction at 11 μm compared to the 12 μm [18]–[20]. Ackerman [18] examined the possibility of using BTD11-12 for dust detection over the Arabian Peninsula, Africa, and the southwest United States. Sokolik [19] conducted a modeling study on the effect of dust on multiple satellite brightness temperatures over water for light and moderate dust loadings of three different mineral compositions. Other studies have also concluded that both polar orbiting imagers such as MODIS [21] and geostationary sensors such as the spinning enhanced visible and infrared imager (SEVIRI) [22], [23] that have the 11 and 12 μm channels can be used to effectively identify dust.

Conversely, the CALIOP CAD algorithm is a multi-dimensional probability distribution function (PDF) approach based on differences in optical and physical properties of clouds and aerosols. The dust is identified from other types of aerosols primarily based on the depolarization ratio. Even though the CAD algorithm has shown success with identifying atmospheric features, such as clouds and aerosols, one of the limitations of the CALIOP is misidentification of dense dust layers as clouds over the Saharan desert [12]. Therefore, in this paper, we use 11 and 12 μm channels from the SEVIRI onboard the Meteosat Second Generation (MSG-2) geostationary platform and Aqua-MODIS to help classify these layers as dust. This is a crucial step since CALIOP data is now being used with CERES to assess the vertical distribution of aerosols and their radiative effects [24].

II. DATA

Table I indicates the satellites used in this study along with some general notes on their associated data products. The CALIPSO satellite flies in formation with a constellation of satellites referred to as the "A-Train" which also includes the Aqua-MODIS and Cloudsat used for this study [25]. Onboard CALIPSO are three different instruments, the CALIOP, the imaging infrared radiometer (IIR), and the wide field camera [26]. The IIR provides measurements collocated with CALIOP at 8.65, 10.6, and 12.05 μm with 1-km spatial resolution. Thus, the IIR measurements could potentially be used in the brightness temperature difference cloud and aerosol discrimination algorithm (BTD CAD) algorithm since it contains spectral bands centered near 11 and 12 μm. In fact, Chen *et al.* [27] has developed an algorithm using the three IIR measurements, and a comparison between their algorithm and the one in this paper will be presented in Section III. However, this study tests the BTD CAD using only MODIS and SEVIRI data because

they provide additional channels that help evaluate the algorithm as discussed later in this section. Therefore, we focus on the CALIOP polarization-sensitive lidar measuring backscatter vertical profiles at 532 and 1064 nm during the day and night which gives information on the vertical location of cloud and aerosols as they have higher backscatter values than the background clear sky [28]. Then, the color ratio [1064/532-nm total attenuated backscatter (AB)] and depolarization ratio (perpendicular/parallel channels at 532 nm) profiles help to distinguish between cloud and aerosol. Clouds generally have larger color ratio values than dust aerosols because 1064- and 532-nm backscatter measurements for clouds are often similar in magnitude due to the larger particles [29]. Depolarization ratio measurements can be used to determine ice-water phase of clouds and aerosol type due to the non-spherical nature of ice and dust particles and more spherical nature of water and smoke particles. However, significant multiple scattering effects occur often with dense water clouds, particularly for space-borne lidars, which leads to much larger depolarization ratios than expected for water clouds [12]. In spite of this, ice clouds are usually associated with the largest depolarization ratios due to the highly non-spherical ice particles.

In order to produce the level 2 CALIPSO product, cloud and aerosol layers are first located using a set of algorithms applied to the level 1 (L1) 532-nm backscatter profiles known as the selective, iterated boundary locater (SIBYL) [13]. SIBYL provides the height of cloud and aerosol layers (physical properties) by scanning CALIOP profiles to detect features, and averaging profiles and removing detected layers from the profiles before further averaging. Features are detected by their return signal being larger than the expected molecular background signal. Then, the cloud and aerosol layer-mean optical properties from layer top to base are computed through the scene classification algorithms. The important level 2 layer-mean optical properties for this study are the 532-nm integrated AB (backscatter), integrated attenuated total color ratio (color ratio), and 532-nm integrated volume depolarization ratio (depolarization ratio). Finally, the PDF-based CAD algorithm is used in the CALIOP production processing to discriminate between clouds and aerosols.

The V1 CAD algorithm uses a 3-D approach taking into account the backscatter, color ratio, and layer center altitude where the PDFs are based on measurements obtained from an airborne lidar and measurements during the lidar in-space technology experiment [29]. With the release of the Version 2 (V2) CAD algorithm came a new set of PDFs based on manual classification of one full day of CALIOP measurements and the incorporation of a new depolarization ratio test which was added to help reduce misclassifications of cloud as aerosol [12]. Even though a noticeable improvement is observed in the V2 CAD algorithm, both Versions 1 and 2 have difficulty distinguishing between aerosol and cloud, particularly optically thick dust and smoke plumes that tend to have very similar scattering properties in the CALIOP channels when compared to clouds [12], [29]. The new V3 product uses a 5-D PDF approach which incorporates the depolarization ratio and latitude along with the backscatter, color ratio, and layer center altitude [30]. Recent tests reveal that the V3 product is significantly more accurate in correctly classifying dense dust and smoke plumes due to the inclusion of the depolarization ratio and latitude [30].

The MSG-2 geostationary satellite carries the SEVIRI multispectral instrument that has a sampling distance of 3 km at subsatellite point and a high temporal resolution of approximately 15 min [31]. MODIS Aqua data are also retrieved for each case study which is a simple task because CALIPSO lags MODIS by only 1.5 min on average as they both fly in the A-Train formation [26]. The MODIS has 36 channels with spatial resolutions ranging from 250 m to 1 km. Finally, we retrieved data from Cloudsat, which flies about 20 s ahead of CALIPSO in the A-Train formation and carries a 94-GHz millimeter-wavelength cloud profiling radar (CPR) with a minimum detectable reflectivity factor near -30 dBZ [32]. Because the signal from the CPR can penetrate clouds which may completely attenuate the CALIOP lidar signal, Cloudsat measurements can be used to confirm cloud thicknesses and to check for additional clouds in these particular regions.

Along with the satellite data sets, the Facility for Airborne Atmospheric Measurements (FAAM) BAE-146 aircraft is used as a validation tool. Various atmospheric and aerosol properties are measured and derived based on the BAE-146 aircraft data, but this study only takes advantage of the 550-nm extinction coefficient data. Johnson *et al.* [33] discusses how the extinction coefficient profiles are retrieved, and Christopher *et al.* [23] uses the profiles to determine the altitude of aerosol layers and estimate the total column AOD. For this study, BAE-146 extinction profiles from the June 21, 2007 dust event over North Africa are used to evaluate level 2 CALIPSO products.

III. Methodology

A. CALIPSO Validation

Fig. 1(a) is a MODIS red-green-blue (RGB) composite image at approximately 1430 UTC on June 21, 2007. NCEP Reanalysis 2.5° by 2.5° 700 hPa wind vectors are shown by white arrows, and the red line depicts the BAE-146 flight path on 21 June with the blue triangle (16.6° N, 16° W) showing the location of a BAE-146 profile from 1402 to 1422 UTC. The black line represents CALIPSO transect with the red section of the line denoting the BTD CAD tested region and white sections denoting the locations of the five cases in Fig. 2(a). The MODIS RGB image clearly shows the advection of thick dust (yellowish color) from the Sahara Desert to the eastern Atlantic Ocean. Adjacent to the southern boundary of the thick dust plume is an extensive area of highly reflective clouds depicted by the green features. Fig. 2(a) shows CALIPSO L1 532 nm AB profiles during its transect on June 21, 2007 at approximately 1440 UTC near the western coast of North Africa. The solid blue and black lines represent MODIS and SEVIRI BTD11-12 values along the CALIPSO transect. Significant differences can exist between the MODIS and SEVIRI BTD11-12 due to the differing spatial and spectral resolutions and spectral response functions of the instruments. Fig. 2(b) shows MODIS (red) and SEVIRI (black) BT11 and MODIS VIS and 0.41 μm (UV) reflectivity depicted by the blue and green lines, respectively. Cloud mask data from the Cloudsat

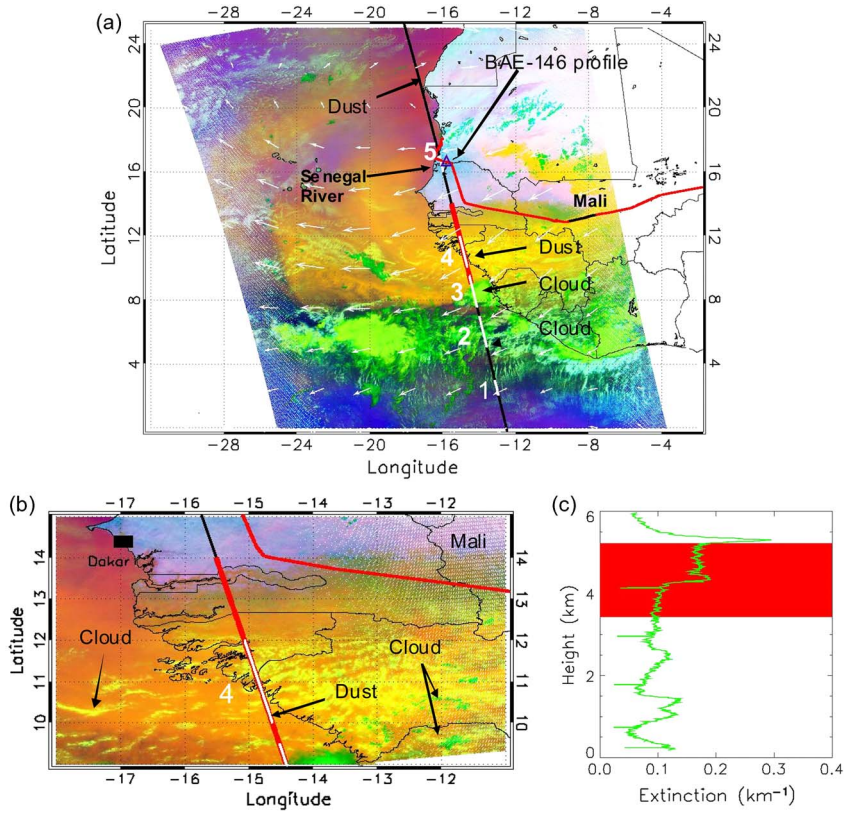

Fig. 1. (a) MODIS RGB composite image at approximately 1430 UTC on 21 June 2007. NCEP Reanalysis 2.5° by 2.5° 700 hPa wind vectors shown by white arrows. Red line depicts BAE-146 flight path on 21 June with the blue triangle (16.6° N, 16° W) showing the location of a BAE-146 profile from 1402 to 1422 UTC. The black line represents CALIPSO transect with the red section of the line denoting the BTD CAD tested region and white sections denoting the locations of the five cases in Fig. 4(a). (b) MODIS RGB image zoomed in on BTD CAD tested region. (c) BAE-146 extinction coefficient profile shown as green. CALIPSO V3 level 2 5 km aerosol and cloud layers detected at approximately 1438 UTC within the column closest to the location of the BAE-146 profile shown as shades of red and blue for aerosol and cloud, respectively.

transect over this same region is displayed in Fig. 2(c). Then, Fig. 3 are scatter plots showing the backscatter, color ratio, and depolarization ratio values for all the cloud and aerosol layers detected by CALIOP within the black box regions numbered 1–5 in Fig. 2(a). These optical properties and classifications are directly from the CALIPSO V3 level 2 5-km layer product where blue and red symbols represent cloud and aerosol layers, respectively. Case 1 represents a light to moderate dust layer with backscatter near 0.003 km^{-1}, color ratio between 0.6 and 0.9, and depolarization ratio between 0.15 and 0.35. The CALIPSO L1 AB profiles suggest the dust is above low-level clouds associated with much larger backscatter values which influenced the strong positive BTD11-12 along this section of the transect. The MODIS RGB image [Fig. 1(a)] shows the dust and low-level cloud from 2 to 3° N by purple and blue colors, respectively. The significant increases in MODIS VIS and UV reflectivity also suggest clouds exist along this portion of the CALIPSO transect. It is worth noting that the low-level clouds are undetected by Cloudsat. The V3 CAD algorithm correctly classifies the Case 1 dust feature because its layer physical and optical properties are very representative of dust and distinguishable from other feature types when using the PDF approach.

The V3 CAD algorithm correctly classifies Case 2, a mid to upper level cloud scene, which appears as a mix of light to bright green colors on MODIS RGB image. In addition to being detected by Cloudsat, Case 2 is associated with significant decreases in BT11 and increases in UV and VIS reflectivity which implies cloud cover. According to Fig. 3, all but two of the cloud layers have CALIPSO optical properties that are separable from the Case 1 dust feature. These are typical optical property values for water clouds as they have larger backscatter and color ratios and lower depolarization ratios than usually retrieved for dust. The other two cloud layers are associated with optical properties very similar to the dust in Case 1. A closer inspection of Fig. 1(a) reveal that these V3 CAD classified cloud layers may actually be remnants of a lofted dust layer adjacent to a water cloud at 8.5 km. It is not often that dust is transported to above 8 km in this geographic region, but the large depolarization ratios along with the sharp increase in collocated BT11 to about 285 K and decrease in BTD11-12 to about 0.5 K suggests dust instead of an ice cloud.

For Case 3, the CALIPSO L1 AB profiles depict high values restricted to the upper troposphere, while Cloudsat detects a very thick cloud extending throughout the troposphere. The CALIPSO L1 AB values are restricted to the upper troposphere because the thick cumulonimbus cloud totally attenuates the CALIOP signal by its topmost 1–2 km part, while the Cloudsat signal is able to penetrate through the cloud. Both the MODIS RGB image reveals the bright green cloud feature which is associated with VIS reflectivity greater than 60% and BT11 below 240 K. Fig. 3 shows that the V3 CAD algorithm accurately

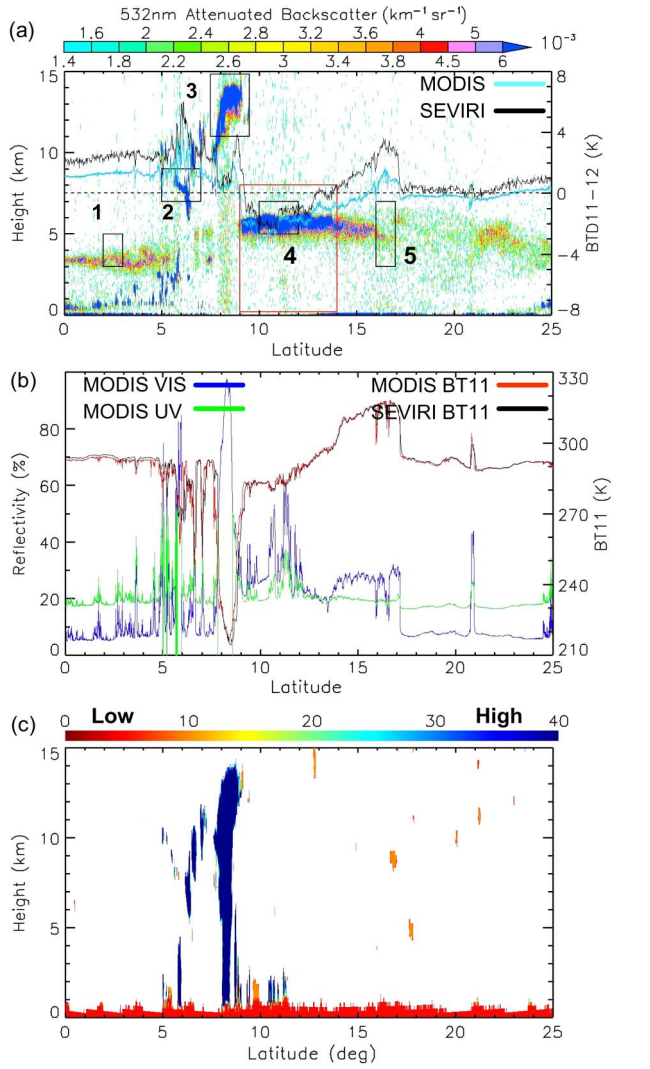

Fig. 2. All panels pertain to the 21 June 2007 case at approximately 1430 UTC. (a) CALIPSO 532 nm L1 AB profiles where the five black boxes denote the location of the cases presented in Fig. 5, while the red box denotes the BTD CAD tested region. Also, MODIS (solid blue line) and SEVIRI (solid black line) BTD11-12 curves are shown. (b) MODIS and SEVIRI BT11 shown by the red and black curves, respectively, and MODIS VIS and UV reflectivity shown by the blue and green curves, respectively. (c) Cloudsat cloud mask with values from 20 to 40 signifying cloud detection. The larger the value, the lower chance of false cloud detection.

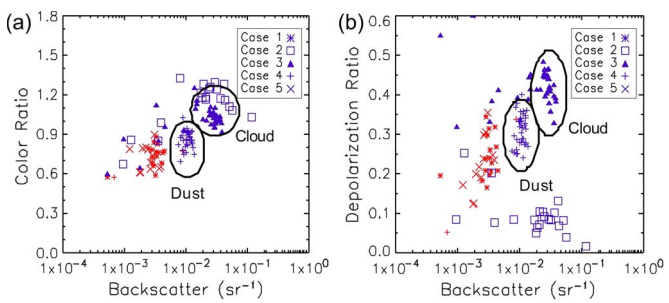

Fig. 3. (a) Scatter plot of CALIPSO V3 level 2 5 km aerosol and cloud backscatter versus color ratio for the five cases numbered 1–5 in Fig. 4(a). Red and blue symbols represent aerosol and cloud, respectively. (b) Same as panel (a) except scatter plot of backscatter versus depolarization ratio. Dust misclassifications are highlighted by the circled area labeled dust, while the true clouds are highlighted by the circled area labeled cloud.

classifies all the CALIPSO detected layers for Case 3 as cloud. With the exception of a couple cloud layers, all the Case 3 layers have optical properties much different than the Case 1 dust plume. This high, thick cloud is clearly composed of numerous ice particles as indicated by the very large depolarization ratios.

The Case 4 region shows L1 AB values larger than 0.006 $km^{-1}sr^{-1}$ and MODIS BTD11-12 between -1 and -3 K which suggests dust. Conversely, Cloudsat detects low-level clouds with high confidence where large increases in UV and VIS reflectivity are also measured. Moreover, the zoomed in MODIS RGB image [Fig. 1(b)] clearly shows a complex scene of thick dust and clouds from 10 to 12° N. CALIPSO L1 AB profiles fail to depict the low-level clouds due to the attenuation of the CALIOP lidar below about 5 km. According to Fig. 3, for Case 4, the V3 CAD algorithm misclassifies the dust as cloud with nearly all the layers having backscatter near 0.01 sr^{-1}, color ratio from 0.6 to 0.9, and depolarization ratio from 0.2 to 0.4. This is an excellent example of a thicker dust layer with optical properties that are more indicative of an ice cloud which causes the V3 CAD misclassifications. In fact, the Case 4 optical properties are close to the values retrieved for the Case 3 ice cloud.

Near coincident CALIPSO and BAE-146 aircraft profiles (16.6° N, 16° W) on 21 June 2007 over North Africa are used to analyze Case 5. Fig. 1(c) shows the BAE-146 aircraft extinction coefficient profile (green line) measured from 1402 to 1422 UTC along with Level 2 5 km CALIPSO aerosol layers detected at approximately 1438 UTC in the column closest to the BAE-146 profile are represented by the red-shaded regions. The CALIPSO V3 CAD algorithm shows a cloud-free atmosphere with an aerosol layer between about 3.5 and 5.5 km which agrees with observations taken along the BAE-146 aircraft profile that determined the region as cloud free. Case 5 backscatter values range from 0.0004 to 0.004 sr^{-1}, depolarization ratio from about 0.12 to 0.35, and color ratio mostly near 0.6, as indicated in Fig. 3. The MODIS RGB image [Fig. 1(a)] supports the BAE-146 observations of a cloud-free atmosphere in the region from 16 to 17° N. Furthermore, the BT11, VIS, and UV spectral curves [Fig. 2(b)] do not indicate any cloud contamination for Case 5 as the significant decreases represented in all the curves are due to CALIPSO transecting over the Senegal River at approximately 16° N. The upper level cloud feature at about 9 km detected with low confidence by Cloudsat is determined as a false detection since none of the other data sources show any indication of clouds from 16 to 17° N. For this relatively light dust region, both MODIS and SEVIRI observe positive BTDs, except for a brief period of negative values observed by MODIS near 16° N. MODIS BTD11-12 is about 2 K less than SEVIRI which is mostly attributed to the fact that Case 5 is primarily over land where the varying surface emissivities throughout the IR can influence significant differences between two satellites that have their own unique spectral response functions for the 11 and 12 μm channels. Conversely, over water, the surface typically does not have a significant impact on BTD11-12 because surface emissivities are very similar throughout the IR spectrum. It is noteworthy that the V2 CAD algorithm misclassifies about 40% of the detected layers for this relatively light dust layer. These

misclassifications are associated with the dust layer above 5 km as the V2 CAD uses stricter thresholds for classifying aerosols at these heights [12]. The V3 results shown here are much improved for Case 5 since it removes the spurious features previously detected as cloud by V2. Thus, the V3 CAD 5-D PDF approach helped greatly to improve the results by classifying an aerosol region that was cloud free according to the validation data.

The solid red box in Fig. 2(a) identifies the most appealing region to test with the BTD CAD algorithm since negative BTD11-12 values are observed along most of this portion of the CALIPSO transect. The V3 CAD algorithm classifies nearly the entire region from 9 to 14° N as cloud, but other data sets used for this study suggest dust resides above lower level cloud. From analyzing the zoomed in MODIS RGB image [Fig. 1(b)] along with the spectral curves and Cloudsat in Fig. 2(b) and (c), it can be concluded that the yellowish features are clouds beneath the dust plume. Moreover, in Fig. 1(b) the BAE-146 is retrieving measurements primarily in Senegal where low-level stratocumulus clouds were observed in the eastern section of the country. The stratocumulus clouds are shown by the green shading along the BAE-146 flight track in eastern Senegal. Making the situation even more complex is the patchy higher level clouds represented by the green features above the thick dust plume from 9 to 12° N. Fig. 2(a) reveals that the CALIOP lidar is able to detect these thin high-level clouds near 12 km at approximately 9.5° N. On the other hand, in Fig. 2(c), Cloudsat fails to detect the thin high-level clouds with any confidence since the clouds are most likely below its minimum detectable signal of about −30 dBZ. Therefore, along this CALIPSO transect, low-level clouds are beneath the dust plume from about 9 to 13° N, while some high-level clouds are present from 9 to 10° N.

B. BTD CAD Algorithm

Fig. 4 shows the flow diagram for BTD CAD developed in this study to improve the CALIOP dust identification. Before applying BTD CAD, a nearest pixel approach is used to locate the closest SEVIRI/MODIS pixel to the CALIPSO footprint. Temporal differences between CALIPSO and SEVIRI/MODIS are not considered by the algorithm since the sampling time differences between the CALIPSO and MODIS Aqua satellites are very small (typically less than 135 s). However, the sampling time differences between the CALIPSO and SEVIRI satellites can be as large as 7 min which may be problematic, particularly in areas of higher wind speeds. After locating the closest SEVIRI/MODIS pixel, the CALIPSO and SEVIRI/MODIS parameters listed in Fig. 4 are extracted and applied to the BTD CAD algorithm. Then, BTD CAD checks whether the CALIPSO feature layer is a cloud. If the layer is a cloud, then BTD CAD continues to consider the feature as a possible misclassification only if BTD11-12 < 0 K and BT11 > 270 K. Negative values of BTD11-12 are typically associated with dust plumes because dust has a larger imaginary index of refraction at 11 μm compared to 12 μm [18]–[20]. Moreover, since the 11 μm and 12 μm channels are rather insensitive to dust composition, a strict BTD11-12 threshold for dust detection can be used [19]. The BT11 threshold is used because most

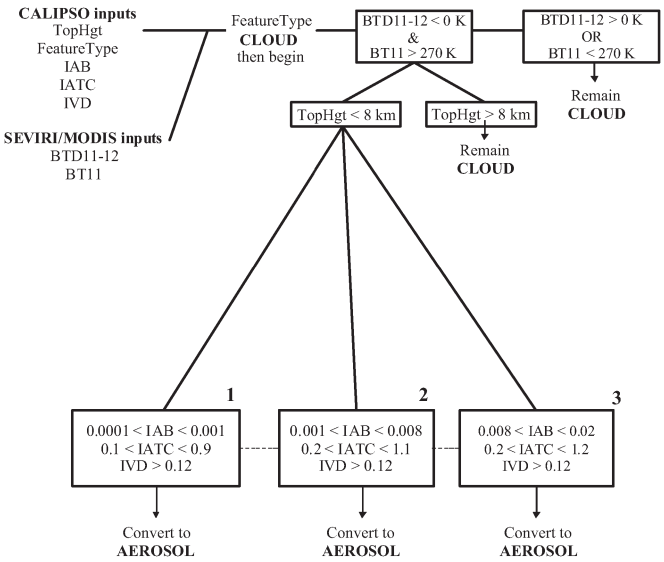

Fig. 4. BTD CAD algorithm flow diagram. IAB refers to the 532-nm integrated attenuated backscatter. IATC refers to the integrated attenuated total color ratio. IVD refers to the 532-nm integrated volume depolarization ratio.

of the V3 CAD dust misclassifications occur near desert source regions where BT11 rarely drops below 270 K. Applying the BT11 threshold helps to minimize the reclassification of true clouds that may be associated with BT11-12 < 0 K. We have observed this particular situation when clouds reside within the same 5-km CALIPSO footprint as aerosol. After that, BTD CAD continues to operate on the cloud feature only if the TopHgt < 8 km since dust aerosol rarely exists above 8 km. The TopHgt is simply the altitude at the top of the aerosol and cloud layers. The TopHgt threshold will prove useful in cases of high cloud edges lying above dust aerosol where BTD11-12 and BT11 fail to reject the cloud. The remaining threshold tests shown by the three boxes in the lower half of Fig. 4 consider the level 2 CALIPSO backscatter, color ratio, and depolarization ratio values (optical properties). If the cloud feature passes all of the optical property tests shown in any one of the three boxes, then the cloud is reclassified as aerosol. If the cloud feature fails the tests, then it remains as cloud. These strict thresholds were developed through close inspection of complex scenes of both cloud and dust where the cloud fails to influence BT11 < 270 K and the dust influences BTD11-12 < 0 K. Finally, CALIPSO uses a horizontal averaging scheme to detect features where lighter features may only be detected when using 20 or 80 km averaging. However, the BTD CAD algorithm operates on 5-km layers. Therefore, if at least one 5-km layer is reclassified as aerosol among a feature detected with 20- or 80-km horizontal averaging, then all the layers associated with that particular feature are reclassified. Section IV will evaluate the validity of the thresholds presented in Fig. 4.

In Fig. 4, we use the same BTD11-12 threshold for both MODIS and SEVIRI even though there is some indication that a slightly higher threshold could be used for SEVIRI. By increasing the SEVIRI threshold to a higher value, such as 0.3 or even 0.5, then many more cloud features will be passed to the TopHgt and optical property tests, which will most likely lead to an increase in true clouds being reclassified as

aerosol. In other words, setting a higher SEVIRI threshold will most likely just decrease the accuracy of the algorithm. Also, the CALIPSO V3 CAD algorithm only misclassifies optically thick dust that is usually always associated with BTD11-12 < 0 K except when optically thick cloud is also present. It is important to note that the optical property test thresholds are determined through examining backscatter, and color and depolarization ratio scatter plots (e.g., Fig. 3) for CALIPSO transects throughout June 2007 over North Africa. The optical property threshold tests along with the TopHgt test help keep true cloud associated with BTD11-12 < 0 K as cloud. Cloud is typically associated with BTD11-12 > 0 K, but there are instances where cloud shows BTD11-12 < 0 K. This most often occurs when cloud and dust exist in the same vertical profile of CALIOP lidar, particularly when low cloud is beneath dust. However, optical property values typical for low-level water clouds are shown in Fig. 3 for Case 2 where depolarization ratio is primarily lower than 0.12. Therefore, the BTD CAD algorithm will keep these as cloud even if a moderate to thick dust plume is present in the same vertical profile which is one of the major strengths of the algorithm. Unfortunately, the significant multiple scattering that can occur within thicker dust plumes can influence unusually high depolarization ratios for low-level water clouds greater than 0.12. When this situation arises, the optical property values for the low-level water clouds can be very similar to dust and can pass the threshold tests 1–3 in Fig. 4. Moreover, another mechanism that can influence low-level water clouds to have similar optical properties as dust is sedimentation and fallout of the dust particles.

Chen *et al.* [24] developed a similar algorithm (CLIM method) to the BTD CAD, but it uses one complex equation involving both a dust index computed through the CALIPSO level 2 layer-mean optical and physical properties and an IR method taking into account the IIR 8.65, 10.60, and 12.05 μm channels in order to separate between features found in the level 2 vertical feature mask (VFM). The CLIM method uses strict coefficients found specifically over the Taklamakan Desert to weight the parameters in the complex equation. Also, noteworthy is the fact that their method only operates on single-layer features in the CALIPSO level 2 VFM mask. Thus, if cloud exists in the same CALIPSO footprint as thick dust, then the CLIM method is unable to detect the dust. On the other hand, the BTD CAD operates only on the CALIPSO level 2 5-km cloud layer product instead of the VFM mask because we are only concerned with converting those misclassified clouds in the cloud layer product into aerosol. Furthermore, the BTD CAD is able to operate on the CALIPSO footprints that contain multiple layers which allows for dust to be detected even in the presence of clouds. Last, the BTD CAD is more versatile than the CLIM method as the CLIM should only be applied over the Taklamakan Desert.

IV. Results and Discussion

A. 21 June 2007 Case

Since the BTD CAD algorithm has now been outlined in Fig. 4, we check how the algorithm would handle the five cases (1–5) on 21 June 2007. Cases 1–3 would fail BTD CAD rather quickly due to positive BTD11-12 collocated with each case which means that the original V3 CAD aerosol and cloud classifications for Cases 1–3 shown in Fig. 3 remain unchanged. Even though BTD CAD will not operate on Cases 1–3, we still check whether the detected layers in each case pass or fail the optical property threshold tests 1–3 in order to check the validity of the thresholds. The Case 1 dust plume passes the threshold tests 1 and 2 in Fig. 4. For Case 2, all but two of the V3 CAD cloud layers fail the optical property tests 1–3 because of low depolarization ratios or high color ratios. The other two cloud layers, which may be associated with a lofted dust layer, fail BTD CAD due to collocated SEVIRI and MODIS BTD11-12 > 0 K and a TopHgt > 8 km. About 10 of the Case 3 cloud layers pass the optical property tests since ice clouds can have similar optical properties as dust. However, the V3 CAD cloud classifications for Case 3 fail BTD CAD due to a TopHgt > 8 km, BTD11-12 > 0 K, and BT11 < 270 K. BTD11-12 nearly becomes negative due to the very thick cloud in the region, which confirms the importance of the BT11 and TopHgt thresholds. Thick clouds with large water contents have high emissivities that are similar at these wavelengths which influence the near negative BTD11-12 values. For Case 4, the V3 CAD misclassifications are converted into aerosols by passing the BTD CAD optical property test 3. Finally, for Case 5, BTD CAD fails immediately due to the positive BTD11-12 except at about 16° N for MODIS. Fortunately, Case 5 is already correctly classified by the V3 CAD. Cases 1–5 suggest that the thresholds used in the BTD CAD algorithm are properly set.

Fig. 5(a) shows CALIPSO L1 AB profiles on June 21 zoomed in on the solid red box in Fig. 2(a). The BTD CAD algorithm results for this same region are presented in Fig. 5(b) and (c) where results using MODIS measurements (MODIS BTD CAD) are in Fig. 5(b) and results using SEVIRI measurements (SEVIRI BTD CAD) are in Fig. 5(c). Fig. 5(b) and (c) indicates the regions of aerosol and cloud within the case study area where Aero and Cld represent unchanged V3 CAD aerosol and cloud layers, while T1–T3 represent the threshold test that the V3 CAD cloud layer passes in order to be converted into an aerosol layer. The solid black lines in Fig. 5(b) and (c) are MODIS and SEVIRI BTD11-12 measurements, respectively, along the CALIPSO transect with the scale ranging from -4 to $+4$ along the right y-axis. Note that the height range is extended up to 15 km in Fig. 5(a) so the high level cloud near 9° N can be seen. SEVIRI BTD CAD is unable to reclassify a couple of these layers that have very similar CALIPSO optical properties as the reclassified layers due to the collocated positive BTD11-12. Thin high-level clouds are most likely influencing the positive SEVIRI BTD11-12 values near 9° N. Conversely, the positive values around 14° N are most likely due to the weakening dust plume as none of the validation data suggests cloud contamination at the latitude. With the exception of the spike in BTD11-12 at 9° N, MODIS measures negative values throughout the entire case study region. One cloud layer near the base of the thick dust plume at about 12° N remains as cloud for both MODIS and SEVIRI BTD CAD due to failing the optical property threshold tests which may be associated with problems correcting the large attenuation of the CALIOP

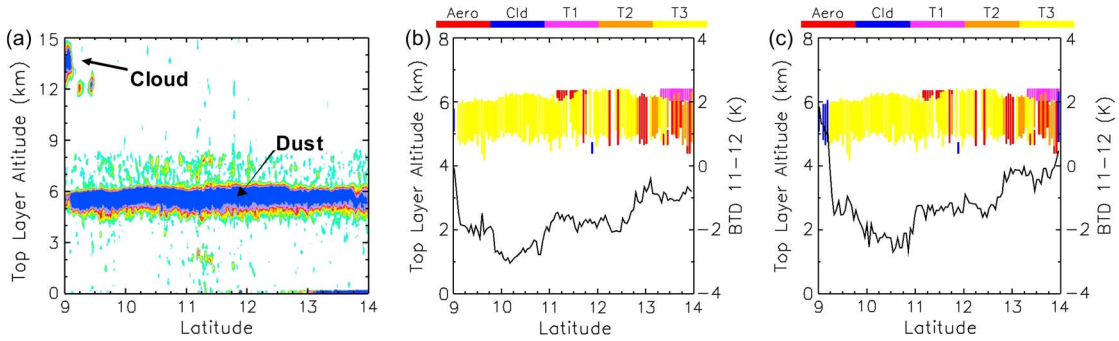

Fig. 5. BTD CAD algorithm results on 21 June 2007 from 9 to 14° N. (a) Close-up of the CALIPSO 532-nm L1 AB profiles over the region of interest using the same scale as Fig. 4(a). Note that the height range is extended up to 15 km in order to depict the high level cloud. (b) MODIS BTD CAD results for the case study area where "Aero" and "Cld" represent unchanged V2 CAD aerosol and cloud layers while "T1–T3" represent the threshold test that the V2 CAD cloud layer passes in order to be converted into an aerosol layer. Thus, "T1–T3" are all aerosol layers. The black solid line shows the BTD11-12 values along the CALIPSO transect with the scale on the right y-axis. (c) Same as panel (b) but for SEVIRI BTD CAD.

lidar signal below about 5 km. In fact, this cloud layer is detected with very low confidence (CALIPSO CAD score < 20) and can be removed from the results. Nevertheless, both the MODIS and SEVIRI BTD CAD overturn previously classified cloud layers associated with a moderately thick dust plume into aerosol. A total of 135 individual 5-km cloud layers are classified by the V3 CAD algorithm from 9 to 14° N while MODIS and SEVIRI BTD CAD reclassify 133 and 131 of these cloud layers, respectively. Most of the layers are converted into aerosol due to the T3 test with some contribution from the T1 and T2 tests where the dust becomes thinner near 14° N.

As mentioned earlier, the V3 CAD algorithm is a 5-D approach which incorporates the depolarization ratio and latitude along with the backscatter, color ratio, and layer center altitude. Unlike the V2 3-D space, dense dust separates well from clouds in the 5-D space. Therefore, the dense dust classification has been improved significantly in the V3 release. However, some misclassifications can still occur when dense or moderately dense dust is transported to high altitudes or high latitudes where cirrus clouds are frequently present [30]. Even though some aerosol layers are reported in the V3 product for this June 21 case, most of the dense dust plume is still misclassified as cloud. A closer look at the V3 browse image (not shown) indicates that these misclassified dust layers are all found at single-shot (0.333 km) or 1-km resolution. Any layers found at 0.333-km resolution are classified as cloud by default without running through the CAD algorithm in the CALIOP Version 1, 2, and 3 releases. If 0.333 km layers are found in a 5-km layer, they will be cleared out from the 5-km layer. Therefore, the 333-m layers will be missed in the 5-km layer product. The misclassification of 1-km dust layers that are run through CAD may be related to the daytime measurement where, as mentioned earlier, SNR is smaller and the color ratio is less accurate due to sunlight induced nonlinear thermal effects which show different latitude dependence for the two wavelength signals. A check of other measurements of the same dust plume acquired during nighttime orbits indicates that the dust can be correctly classified in these nighttime CALIOP measurements except the part found at 0.333-km resolution. This may indicate a need for further optimization of the 5-D PDFs to account for the day and night differences. Although the V3 CALIPSO CAD algorithm is much improved, it still encounters problems with

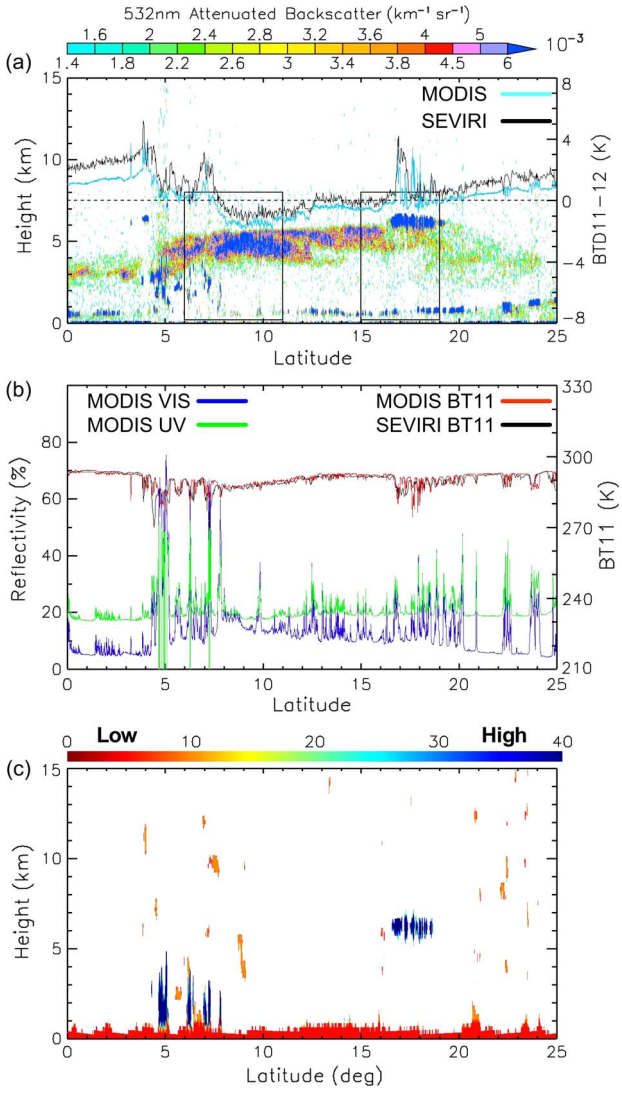

Fig. 6. Same panels as shown in Fig. 4 but for the 22 June 2007 case at approximately 1515 UTC. The two solid black boxes in panel (a) denote the regions where the BTD CAD algorithm is applied.

classifying some optically thick dust at higher altitudes and the BTD CAD algorithm can help negate these problems. More importantly, the BTD CAD algorithm can help classify the

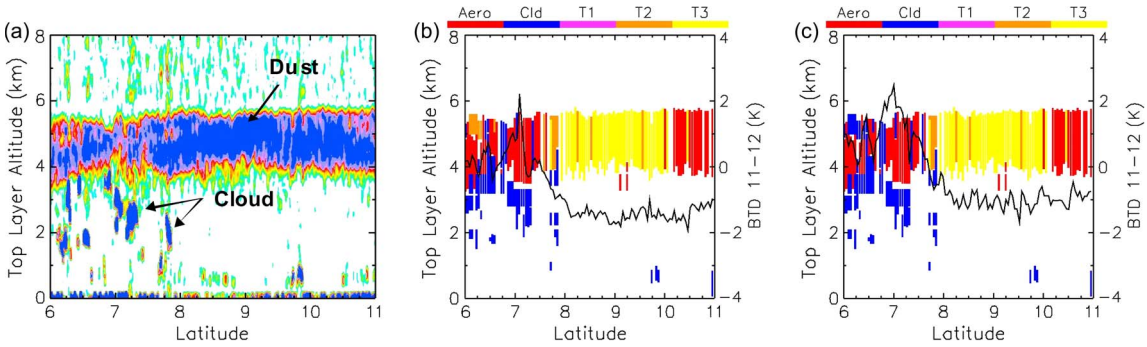

Fig. 7. Same panels as Fig. 5 but BTD CAD results for the 22 June 2007 case from 6 to 11° N.

misclassified dust layers found at 0.333 km. As mentioned earlier, the CALIOP scene classification identifies all 0.333-km layers as cloud by default. As demonstrated by this case, very dense regions of a dust plume can be found frequently at 0.333-km resolution and consequently misclassified as cloud. These very dense dust layers fall in a region that the BTD CAD algorithm can confidently classify.

B. 22 June 2007 Case

The June 22, 2007 case is another very challenging test for the BTD CAD algorithm as both low and mid-level clouds exist with the dust plume, which is the same plume from June 21 but transported westward over the Atlantic Ocean. We followed this dust plume in order to test the ability of the BTD CAD algorithm over an ocean region away from the dust source region. Additionally, this case proves that the V3 CAD algorithm encounters issues with classifying dust over areas other than the dust source regions if the dust remains optically thick after a long-distance transport. Fig. 6 is the same as Fig. 2 except that it is for June 22, 2007 at approximately 1515 UTC. The two solid black boxes in Fig. 6(a) denote the regions where the BTD CAD algorithm is applied and CALIPSO L1 AB profiles suggest low-level clouds are present in both regions. Cloudsat shows no confidence in detecting any of the low-level clouds. At the same time, the MODIS VIS and UV spectral curves in Fig. 6(b) clearly suggest cloud contamination along the entire CALIPSO transect with significant increases occurring with the low-level clouds in the black box regions. A comparison between Figs. 2(a) and 6(a) show a decrease in L1 AB values and increase in BTD11-12 with this dust plume which suggests the plume weakened over the past 24 h. Even though the plume weakened, the V3 CAD algorithm still classifies a significant portion of the dust as cloud. MODIS measures negative BTD11-12 throughout most of the dust, except for areas contaminated with thicker cloud. In the thinner region of the dust plume from 13 to 17° N, SEVIRI primarily measures slightly positive BTD11-12 while MODIS shows slightly negative values.

Fig. 7 presents MODIS and SEVIRI BTD CAD results for the region from 6 to 11° N. From 6° N to about 8° N, MODIS VIS and UV reflectivity curves show some reflectance values above 40%. Cloudsat appears to detect these higher reflective clouds better than CALIPSO as the cloud thicknesses are about 2–3 km according to Cloudsat while the CALIOP lidar signal experiences strong attenuation from the clouds. Then, the region from 8 to 11° N is dominated by dust and much thinner low-level clouds. The thinner low-level clouds are clearly revealed by the MODIS RGB composite image (not shown). The CALIOP signal again appears to undergo significant attenuation, particularly from 8 to 10° N, which is indicated by the reduction of a surface signal in this particular region and inability to detect some of the low-level clouds. As shown in Fig. 7, both MODIS and SEVIRI BTD CAD reclassify many of the V3 CAD misclassifications associated with the dust plume from 4 to 6 km as aerosol. From about 6 to 8° N, misclassifications are still shown with this dust plume due to the thicker clouds influencing positive BTD11-12 in this region. Overall, the results are encouraging as MODIS and SEVIRI BTD CAD convert 62 and 54 cloud layers into aerosol, respectively. Perhaps even more encouraging is the fact that the clouds beneath the portions of the dust plume associated with negative BTD11-12 remain as cloud because they fail the optical property threshold tests within the BTD CAD algorithm. This shows the necessity of the optical property threshold tests and suggests that proper thresholds are set within BTD CAD. These clouds fail the optical property tests due to color ratios higher than the maximum threshold, while two layers also have depolarization ratios lower than the minimum threshold (not shown). Most of the misclassified layers are converted into aerosol due to the T3 test. In the thinner portion of the dust plume from 6 to 8° N, the T2 test is the main contributor. We also test the BTD CAD algorithm on the region denoted by the black box in Fig. 6(a) from 15 to 19° N, and the results are also good as the mid-level and low-level cloud layers remain as cloud while the misclassified dust layers are reclassified as aerosol (not shown).

TABLE II
TOTAL NUMBER OF AEROSOL LAYERS DETECTED BY V2 CAD, MODIS V2, V3 CAD, AND MODIS V3 IN THE 0–2, 2–4, 4–6, AND 6–8 km HEIGHT BINS FOR ALL DAYTIME CALIPSO TRANSECTS DURING JUNE 2007. MODIS V2 AND V3 REFER TO MODIS BTD CAD APPLIED TO THE V2 AND V3 DATA

Height Bin	V2 CAD	MODIS V2	V3 CAD	MODIS V3
0-2 km	7130	7611	8039	8089
2-4 km	22488	23411	14745	14773
4-6 km	18234	20488	18854	18998
6-8 km	268	1217	1468	1628

C. V2 Versus V3

MODIS BTD CAD is applied to all daytime CALIPSO transects over North Africa (0–25° N, 25° E–20° W) during June 2007, and the total number of detected aerosol layers in each height bin are presented in Table II. The original CALIPSO V2 and V3 CAD algorithm results are shown in the V2 CAD and V3 CAD columns, respectively. We also apply the MODIS BTD CAD to the CALIPSO V2 and V3 CAD algorithms and the results are shown in the MODIS V2 and MODIS V3 columns. Table II is separated by height bins according to the top height directly from the CALIPSO level 2 layer product. Thus, if the aerosol layer has a top height of 3 km, then it is counted in the 2–4 km height bin. Not surprisingly, the majority of the reclassifications for both MODIS V2 and MODIS V3 occur in the 6–8 km height bin since the CALIPSO CAD algorithms use more conservative thresholds at these heights due to the fact that aerosols are infrequently lifted above 6 km [12]. The conservative thresholds can cause thick dust layers to be misclassified as cloud when they reach these heights. The June 21, 2007 case is an excellent example of dust misclassifications occurring above 6 km. Overall, the increase in the total number of aerosol layers in each height bin is much smaller when comparing V3 CAD and MODIS V3 as opposed to V2 CAD and MODIS V2, which can be credited to the replacement of the previous 3-D PDF approach with the 5-D PDF approach. This much closer agreement between the V3 CAD and MODIS V3 results for each height bin proves the 5-D PDF approach is much more accurate compared to the 3-D PDF approach. V3 CAD does very well with classifying aerosol layers between 0 and 6 km as very minimal differences occur between V3 CAD and MODIS V3.

V. Conclusion

This study proposed an algorithm (BTD CAD) that uses multi-spectral satellite measurements along with the CALIPSO layer optical properties to improve the classification accuracy of the V3 CAD algorithm. Because the BTD CAD algorithm only utilizes the 11 and 12 μm infrared channels, it can operate during the day and night. The ability of BTD CAD was tested on more than a dozen dust plume cases measured by the CALIPSO satellite over North Africa and the eastern Atlantic Ocean during June 2007. Results from two of the more difficult and interesting dust plume cases are presented in this paper. A thorough validation of the results is conducted using a combination of CALIPSO L1 AB profiles, the Cloudsat cloud mask, spectral signatures, and RGB composite images. The V3 CAD algorithm performed poorly in each of these cases as the dust aerosols were frequently misclassified as clouds. Conversely, BTD CAD performed very well in each of the cases as many of the V3 CAD misclassifications were correctly reclassified into aerosol. We also clearly showed that only using BTD11-12 to correct dust misclassifications will often lead to true clouds being reclassified into aerosol. Sometimes, clouds can be associated with negative BTD11-12, particularly when both dust and cloud are present in the same atmospheric column, and CALIPSO can detect multiple layers in a single profile. The additional threshold tests within BTD CAD help mitigate the problem of clouds being associated with negative BTD11-12. Although the V3 CAD algorithm significantly reduces the dust misclassifications observed in the V2 release, we showed that the BTD CAD algorithm can still help in the regions of optically thick dust at higher altitudes where the V3 CAD classifies cloud.

However, the BTD CAD is not without its flaws as there can be instances where clouds associated with negative BTD11-12 pass the additional threshold tests and are consequently converted into aerosol layers. This can occur where low-level water clouds reside beneath thick dust because the significant multiple scattering occurring within the dust layer can lead to unusually large depolarization ratios for the water clouds which usually have low depolarization values. The unusually large depolarization ratios can be similar to that observed in dust layers. Also, the BTD CAD is unable to reclassify a misclassified dust layer when BTD11-12 is positive which most often occurs when clouds exist in the same column as dust. We show several instances of this occurrence in the case studies presented. Futhermore, the BTD CAD uses a strict BTD11-12 threshold of 0 K even though spectral emissivities can vary significantly between different surface types which impact the observed BTD11-12. This suggests that the surface emissivity should be taken into account instead of using direct BTDs. However, we do not believe this will lead to substantial improvements because the V3 CALIPSO CAD algorithm only shows misclassifications with thick dust. When thick dust is present, the surface effects on the BTD11-12 will be minimized. Nevertheless, it would be interesting to check the impact of including the surface emissivity on the BTD CAD algorithm. Finally, this study tests the BTD CAD algorithm for cases over one region in June 2007 where good results were shown. Additional case studies near dust source regions need to be analyzed in order to further validate the accuracy of the algorithm. In particular, more case studies where both cloud and aerosol are present need to be assessed due to complex vertical alignments of cloud and aerosol that can exist in the atmosphere.

In addition to proposing an algorithm that shows great potential in further improving the classification accuracy of the V3 CAD algorithm, we assessed the strength of the MODIS and SEVIRI satellites in detecting dust since both of their measurements were used in the BTD CAD algorithm. For the two case studies, MODIS BTD CAD performed better than SEVIRI BTD CAD which is mostly attributed to the increased sensitivity of the MODIS BTD11-12 to dust aerosol. In particular, negative MODIS BTD11-12 is often observed in regions of lighter dust where SEVIRI BTD11-12 is often positive. Additionally, the higher spatial resolution of MODIS appears to positively impact the BTD CAD results, which is particularly noticeable in complex regions of cloud and dust and near cloud-aerosol boundaries where SEVIRI tends to observe all positive BTD11-12 while MODIS observes areas of negative BTD11-12. Furthermore, the temporal differences between these satellites are only briefly mentioned in this study and are not taken into account by BTD CAD. The temporal differences between MODIS and CALIPSO are minimal since

they both fly in the A-Train of satellites. On the other hand, a 5 or 6-min difference can exist between SEVIRI and CALIPSO sampling times which may cause problems with the SEVIRI BTD CAD algorithm. However, this temporal difference did not appear to significantly impact the SEVIRI BTD CAD results for the two case studies. Our study clearly indicates that multi-sensor approaches are beneficial for aerosol studies as opposed to using single sensors alone.

ACKNOWLEDGMENT

The MODIS data were obtained through the Goddard Distributed Active Archive Center. Special thanks to Ben Johnson foe the FAAM aircraft data.

REFERENCES

[1] P. Forster, V. Ramaswamy, P. Artaxo, T. Berntsen, R. Betts, D. W. Fahey, J. Haywood, J. Lean, D. C. Lowe, G. Myhre, J. Nganga, R. Prinn, G. Raga, M. Schulz, and R. Van Dorland, "Changes in atmospheric constituents and in radiative forcing," in *Climate Change 2007—The Physical Science Basis. Contribution of Working Group I to the Fourth Assessment Report of the Intergovernmental Panel on Climate Change*, S. Solomon, D. Qin, M. Manning, Z. Chen, M. Marquis, K. B. Averyt, M. Tignor, and H. L. Miller, Eds. New York: Cambridge Univ. Press, pp. 131–217.

[2] Y. J. Kaufman, D. Tanré, and O. Boucher, "A satellite view of aerosols in the climate system," *Nature*, vol. 419, pp. 215–223, Sep. 2002.

[3] J. M. Haywood and O. Boucher, "Estimates of the direct and indirect radiative forcing due to tropospheric aerosols: A review," *Rev. Geophys.*, vol. 38, no. 4, pp. 513–543, Nov. 2000.

[4] J. L. Zhang and S. A. Christopher, "Longwave radiative forcing of Saharan dust aerosols estimated from MODIS, MISR, CERES observtions on Terra," *Geophys. Res. Lett.*, vol. 30, no. 23, p. 2188, 2003. doi:10.1029/2003GL018479.

[5] E.-S. Yang, P. Gupta, and S. A. Christopher, "Net radiative effect of dust aerosols from satellite measurements over Sahara," *Geophys. Res. Lett.*, vol. 36, no. 18, pp. L18 812-1–L18 812-5, 2009. doi:10.1029/2009GL039801.

[6] S. Twomey, "The infuence of pollution on the shortwave Albedo of clouds," *J. Atmos. Sci.*, vol. 34, no. 7, pp. 1149–1152, 1977.

[7] J. Su, J. Huang, Q. Fu, P. Minnis, J. Ge, and J. Bi, "Estimation of Asian dust aerosol effect on cloud radiation using Fu-Liou radiative model and CERES measurements," *Atmos. Chem. Phys.*, vol. 8, no. 10, pp. 2763–2771, 2008.

[8] S. A. Christopher, J. Zhang, Y. J. Kaufman, and L. A. Remer, "Satellite-based assessment of top of atmosphere anthropogenic aerosol radiative forcing over cloud-free oceans," *Geophys. Res. Lett.*, vol. 33, no. 15, pp. L15 816-1–L15 816-4, Aug. 2006. doi:10.1029/2005GL025535.

[9] S. A. Christopher and T. Jones, "Satellite-based assessment of cloud-free net radiative effect of dust aerosols over the Atlantic Ocean," *Geophys. Res. Lett.*, vol. 34, no. 2, pp. L02 810-1–L02 810-4, 2007. doi:10.1029/2006GL027783.

[10] F. Patadia, E.-S. Yang, and S. A. Christopher, "Does dust change the clear sky top of atmosphere shortwave flux over high surface reflectance regions?," *Geophys. Res. Lett.*, vol. 36, no. 15, pp. L15 825-1–L15 825-5, 2009. doi:10.1029/2009GL039092.

[11] D. Chand, R. Wood, T. L. Anderson, S. K. Satheesh, and R. J. Charlson, "Satellite-derived direct radiative effect of aerosols dependent on cloud cover," *Nature Geosci.*, vol. 2, no. 3, pp. 181–184, Mar. 2009.

[12] Z. Liu, M. A. Vaughan, D. M. Winker, C. Kittaka, B. Getzewich, R. Kuehn, A. Omar, K. A. Powell, C. Trepte, and C. A. Hostetler, "The CALIPSO lidar cloud and aerosol discrimination: Version 2 algorithm and initial assessment of performance," *J. Atmos. Ocean. Technol.*, vol. 26, no. 7, pp. 1198–1213, Jul. 2009.

[13] D. M. Winker, M. A. Vaughan, A. Omar, Y. Hu, K. A. Powell, Z. Liu, W. H. Hunt, and S. A. Young, "Overview of the CALIPSO mission and CALIOP data processing algorithms," *J. Atmos. Ocean. Technol.*, vol. 26, no. 11, pp. 2310–2323, Nov. 2009.

[14] W. H. Hunt, D. M. Winker, M. A. Vaughan, K. A. Powell, P. L. Lucker, and C. Weimer, "CALIPSO lidar description and performance assessment," *J. Atmos. Ocean. Technol.*, vol. 26, no. 7, pp. 1214–1228, Jul. 2009.

[15] K. A. Powell, C. A. Hostetler, Z. Liu, M. A. Vaughan, R. E. Kuehn, W. H. Hunt, K.-P. Lee, C. R. Trepte, R. R. Rogers, S. A. Young, and D. M. Winker, "CALIPSO lidar calibration algorithms. Part I: Nighttime 532-nm parallel channel and 532-nm perpendicular channel," *J. Atmos. Ocean. Technol.*, vol. 26, no. 10, pp. 2015–2033, Oct. 2009.

[16] M. A. Vaughan, Z. Liu, M. J. McGill, Y. Hu, and M. D. Obland, "On the spectral dependence of backscatter from cirrus clouds: Assessing CALIOP's 1064 nm calibration assumptions using cloud physics Lidar measurements," *J. Geophys. Res.*, vol. 115, no. 14, pp. D14 206-1–D14 206-17, 2010. doi:10.1029/2009JD013086.

[17] R. V. Cakmur, R. L. Miller, J. Perlwitz, I. V. Geogdzhayev, P. Ginoux, D. Koch, K. E. Kohfeld, I. Tegen, and C. S. Zender, "Constraining the magnitude of the global dust cycle by minimizing the difference between a model and observations," *J. Geophys. Res.*, vol. 111, no. D6, pp. D06 207-1–D06 207-24, 2006. doi:10.1029/2005JD005791.

[18] S. A. Ackerman, "Remote sensing aerosol using satellite infrared observations," *J. Geophys. Res.*, vol. 102, no. D14, pp. 17 069–17 079, 1997. doi:10.1029/96JD03066.

[19] I. N. Sokolik, "The spectral radiative signature of wind-blown mineral dust: Implications for remote sensing in the thermal IR region," *Geophys. Res. Lett.*, vol. 29, no. 24, pp. 2154–2157, 2002.

[20] J. P. Chaboureau, P. Tulet, and C. Mari, "Diurnal cycle of dust and cirrus over West Africa as seen from meteosat second generation satellite and a regional forecast model," *Geophys. Res. Lett.*, vol. 34, no. 2, pp. L02 882-1–L02 882-5, 2007. doi:10.1029/2006GL027771.

[21] A. Darmenov and I. N. Sokolik, "Identifying the regional thermal-IR radiative signature of mineral dust with MODIS," *Geophys. Res. Lett.*, vol. 32, no. 16, pp. L16 803-1–L16 803-5, 2005. doi:10.1029/2005GL023092.

[22] H. E. Brindley, "Estimating the top of atmosphere longwave radiative forcing due to Saharan dust from satellite observations over a West African site," *Atmos. Sci. Lett.*, vol. 8, no. 3, pp. 74–79, Jul./Sep. 2007.

[23] S. A. Christopher, B. Johnson, T. A. Jones, and J. Haywood, "Vertical and spatial distribution of dust from aircraft and satellite measurements during the GERBILS field campaign," *Geophys. Res. Lett.*, vol. 36, no. 6, pp. L06 806-1–L06 806-5, Mar. 2009. doi:10.1029/2008GL037033.

[24] J. Huang, Q. Fu, J. Su, Q. Tang, P. Minnis, Y. Hu, Y. Yi, and Q. Zhao, "Taklimakan dust aerosol radiative heating derived from CALIPSO observations using the Fu-Liou radiation model with CERES constraints," *Atmos. Chem. Phys.*, vol. 9, no. 12, pp. 4011–4021, Jul. 2009.

[25] G. L. Stephens, D. G. Vane, R. J. Boain, G. G. Mace, K. Sassen, Z. Wang, A. J. Illingworth, E. J. O'Connor, W. B. Rossow, S. L. Durden, S. D. Miller, R. T. Austin, A. Benedetti, and C. Mitrescu, "THE cloudsat mission and the A-Train," *Bull. Amer. Meteorol. Soc.*, vol. 83, no. 12, pp. 1771–1790, Dec. 2002.

[26] D. M. Winker, J. R. Pelon, and M. P. McCormick, "The CALIPSO mission: Spaceborne lidar for observation of aerosols and clouds," in *Proc. SPIE*, 2003, vol. 4893, pp. 1–11.

[27] B. Chen, J. Huang, P. Minnis, Y. Hu, Y. Yi, Z. Liu, D. Zhang, and X. Wang, "Detection of dust aerosol by combining CALIPSO active lidar and passive IIR measurements," *Atmos. Chem. Phys.*, vol. 10, no. 9, pp. 4241–4251, May 2010.

[28] M. Vaughan, S. Young, D. Winker, K. Powell, A. Omar, Z. Liu, Y. Hu, and C. Hostetler, "Fully automated analysis of space-based lidar data: An overview of the CALIPSO retrieval algorithms and data products," in *Proc. SPIE*, 2004, vol. 5575, pp. 16–30.

[29] Z. Liu, M. A. Vaughan, D. M. Winker, C. A. Hostetler, L. R. Poole, D. Hlavka, W. Hart, and M. McGill, "Use of probability distribution functions for discriminating between cloud and aerosol in lidar backscatter data," *J. Geophys. Res.*, vol. 109, no. D15, pp. D15 202-1–D15 202-13, 2004. doi:10.1029/2004JD004732.

[30] Z. Liu, R. Kuehn, M. Vaughan, D. Winker, A. Omar, K. Powell, C. Trepte, Y. Hu, and C. Hostetler, "The CALIPSO cloud and aerosol discrimination: Version 3 algorithm and test results," presented at the Proc. 25th ILRC, St. Petersburg, Russia, 2010.

[31] J. Schmetz, P. Pili, S. Tjemkes, D. Just, J. Kerkmann, S. Rota, and A. Ratier, "An introduction to meteosat second generation (MSG)," *Bull. Amer. Meteorol. Soc.*, vol. 83, no. 7, pp. 977–992, Jul. 2002.

[32] R. Marchand, G. G. Mace, T. Ackerman, and G. Stephens, "Hydrometer detection using cloudsat—An earth-orbiting 94-GHz cloud radar," *J. Atmos. Ocean. Tech.*, vol. 25, no. 4, pp. 519–533, Apr. 2008.

[33] B. T. Johnson, S. A. Christopher, J. M. Haywood, and S. R. Osborne, "Measurements of aerosol properties from aircraft, satellite and ground-based remote sensing: A case study from the dust and biomass burning experiment (DABEX)," *Q. J. R. Meteorol. Soc.*, vol. 135, no. 641, pp. 922–934, Apr. 2009.

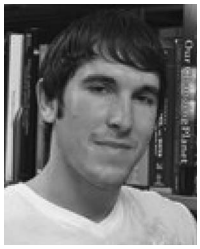

Aaron R. Naeger received the B.S. degree in atmospheric science from the Univerisity of Missouri, Columbia, MO, in 2007, and the master's degree from the University of Alabama, Huntsville, in 2010, where he is currently working toward the Ph.D. degree in the Department of Atmospheric Science, with Dr. Sundar Christopher as his advisor. His Ph.D. research focuses on the dust aerosol impacts on tropical cyclone formation and development where he is using multisensory satellite observations along with radiative transfer and mesoscale modeling to help improve forecasts for tropical cyclones.

His primary research interests include satellite remote sensing of clouds and aerosols, and radiative transfer and mesoscale modeling. Currently, he is the lead author of one and coauthor of two peer-reviewed publications.

Sundar A. Christopher received the Ph.D. degree in atmospheric sciences from Colorado State University, Fort Collins, in 1995. He also holds the M.S. degree in meteorology from the South Dakota School of Mines and Technology, Rapid, South Dakota, and the M.S. degree in industrial/organizational psychology from the University of Alabama, Huntsville.

He is a Professor and Chairman of the Department of Atmospheric Science at the University of Alabama, Huntsville, where he also serves as the Associate Director of the Earth System Science Center. His research interests include satellite remote sensing of clouds and aerosols and their impact on air quality, environment, health, and global and regional climate. He enjoys teaching and has designed a professional development course for graduate students. His recently published book, *Navigating Graduate School and Beyond: A Career Guide for Graduate Students*, incorporates ideas from this course. He has published more than 100 papers in peer-reviewed journals and has presented his work at major scientific conferences, universities, and other organizations across the globe.

Richard Ferrare (M'01) is a Senior Research Scientist in the Atmospheric Composition Branch, Science Directorate, at the NASA Langley Research Center. From 1985 to 1988, he worked in the Climate and Radiation Branch at NASA/Goddard Space Flight Center (GSFC) where he investigated atmospheric aerosol optical, and physical properties using satellite and ground-based measurements. Between 1988 and 1991, he developed the algorithms and software needed to retrieve atmospheric water vapor, temperature, and aerosol scattering and extinction from data collected by the GSFC Scanning Raman Lidar system. He also developed the algorithms and software used to derive ozone, temperature, and aerosol profiles from data collected by the GSFC stratospheric DIAL ozone lidar. He has extensive experience in the acquisition and analyses of atmospheric remote sensing data, and in particular, lidar data. He has participated in many field experiments with NASA ground-based and airborne lidar systems. He has developed and used algorithms to retrieve aerosol backscattering and extinction profiles using data acquired by the Department of Energy Atmospheric Radiation Measurement (ARM) Program Southern Great Plains Raman Lidar. He was the Chairman of the DOE ARM Aerosol Working Group (2000 to 2004) and a member of the ARM Climate Research Facility Science Board. He was the Chief Scientist for the May 2003 Aerosol Intensive Operations Period held at the ARM SGP site and was the Coordinator of the *JGR-Atmospheres* Special Section that presented the results of this mission. He has been the Principal Investigator on NASA and DOE ARM projects related to ground-based Raman and airborne lidar studies of aerosols and water vapor, as well as NASA EOS investigations. He has been a member of the MODIS and CALIPSO science teams.

Dr. Ferrare is a member of the American Geophysical Union, Optical Society of America, Engineers, and the American Meteorological Society. He is author or coauthor of 92 peer-reviewed publications (13 as lead author).

Zhaoyan Liu (M'07) received the B.E. degree in laser physics, in 1984, and the M.E. degree in optics from the Harbin Institute of Technology, Harbin, China, in 1987, and the D.E. degree in system design from Fukui University, Fukui, Japan, in 1996.

Currently, he is a Lead Research Scientist with Science Systems and Applications, Inc., Hampton, VA, and has been a member of the Lidar Science Working Group of the NASA-CNES joint CALIPSO satellite mission since 2001. His research interests include laser and lidar system development and lidar remote sensing.

Dr. Liu is a member of American Geophysical Union.